Journal of the European Ceramic Society 17 (1997) 681–688

PII: S0955-2219(96)00086-6
0955-2219/97/$17.00

Statistical Evaluation of Corrosion of Sialon in Burner Rig Simulated Combustion Atmospheres

K. G. Ahari,[a] K. S. Coley[a,*] & J. R. Nicholls[b]

[a]Metallurgy and Engineering Materials Group, Department of Mechanical Engineering, University of Strathclyde, Glasgow G1 1XN, UK
[b]School of Industrial and Manufacturing Science, Cranfield University, Cranfield, Bedfordshire, MK43 0AL, UK

(Received 30 November 1995; revised version received 3 April 1996; accepted 3 May 1996)

Abstract

Samples of a sialon with low levels of aluminium substitution were exposed, for times up to 500 h, to a combustion atmosphere simulated in a low-velocity burner rig at 1300°C. Corrosion was evaluated by metallographic measurement of multiple polished sections. It was found that the extent of corrosion varied systematically along the length of each sample, which has been explained as being the result of creep of the corrosion scale towards the base of the sample. The data from a number of measurement points along a sample were combined using a normalizing procedure so that a sufficiently large data set could be acquired for statistical analysis. Extreme value statistics were used to analyse the section loss data and the extreme value parameters μ_e and σ_e were determined and correlated with time of exposure. The most likely extreme value, μ_e, was found to follow a parabolic relationship with time which is in conflict with mass change results, where the parabolic rate constant decreased at longer times. The time-dependent correlation for the extreme value parameters was used, in conjunction with the reproductive property of the extreme value model, to predict the most likely maximum extreme value at longer times and for larger sample sizes. The results of this prediction were compared with data for superalloys corroded in similar atmospheres at 900°C. The behaviour of the sialon was found to be comparable with that of uncoated superalloys. © *1997 Elsevier Science Limited. All rights reserved.*

Introduction

Sialons and silicon nitride have very good high-temperature mechanical properties, and therefore are candidate materials for use in a number of combustion applications[1,2] where they are likely to be exposed to a wide range of corrosive species. It is therefore essential that reliable corrosion data are obtained in order to assess the suitability of these materials for particular applications.

The major cause of corrosion in metallic gas turbines is sodium sulfate, which deposits on components and reacts with the protective oxide scale thereby reducing its protectiveness.[3–5] Corrosion of silicon-based ceramics by molten salts has been studied by a number of workers,[6–8] and has been shown to follow similar principles to the corrosion of alloys. However, there have been relatively few studies on corrosion above the dew point of these salts,[9,10] which are likely to be representative of the service temperatures of ceramic components. The present study examines the behaviour of sialon and sintered silicon nitride in a sodium- and sulfur-bearing combustion atmosphere at temperatures above the dew point of sodium sulfate.

Burner rig testing has been found to be the most effective way of simulating gas turbine corrosion in the laboratory,[11,12] although in early intercomparisons between different laboratories, there was a large degree of scatter in the reported corrosion rates.[13] It was suggested by Hancock[14] that these differences were caused by different contaminant flux rates (CFRs). Saunders *et al.*[15] proposed that deposition rate was more critical but conceded that this was more difficult to control than CFR, and a more recent comparison showed reasonable agreement between burner rigs operated at similar CFRs.[16] A recent VAMAS round robin[17] was based on the concept that deposition rate/CFR is the critical parameter, and a number of high- and low-velocity rigs were compared on this basis at 700°C and 900°C. The VAMAS round robin gave a much tighter spread of results, particularly when low- and high-velocity rigs were considered separately. The discrepancies between rigs, and in particular between high- and

*To whom correspondence should be addressed.

low-velocity rigs, were attributed to large differences in the deposition rates despite similar CFRs. Saunders and Nicholls concluded that, in order to obtain reliable comparisons between different burner rigs, deposition rate must be controlled. The present work used the CFR proposed for the VAMAS round robin,[18] in a burner rig of identical configuration to Laboratory 1 in Ref. 17. In this way, it is believed that the behaviour of the ceramic materials studied here can be compared with the performance of metallic materials tested by Laboratory 1 in the VAMAS round robin, although it is accepted that contaminant flux rate may not be a critical parameter at temperatures above the dew point of sodium sulfate.

There are a number of ways of measuring corrosion, the most popular of which is by mass change. This method is simple and relatively cheap to carry out, but only provides information on the average corrosion rate. This may well be sufficient for many purposes and can give useful mechanistic information, as well as providing an insight into the effect of various parameters on the corrosion process. Mass change results from this study have been reported elsewhere[10,19] and have been used to investigate the corrosion mechanisms. However, the current work seeks to assess the maximum extent of corrosion, which will ultimately be the cause of component failure and is therefore of most interest when selecting materials for service.

Nicholls and Hancock[20] have suggested that the maximum observed corrosion may not be the true maximum, as this depends on sectioning the sample at the point where maximum corrosion occurs. They therefore proposed the use of extreme value statistics to predict the most likely maximum from analysis of a number of section loss measurements. This technique has been employed in the present study to predict the most likely maximum.

Experimental

Cylindrical section samples of a sialon, material A, of composition shown in Table 1, were exposed in a low-velocity burner rig for times up to 500 h. The configuration of the rig is identical to that used in Laboratory 1 reported in the recent VAMAS round robin, with the additional feature that the present rig has a higher temperature capability. A schematic diagram of the burner rig is shown in Fig. 1. Although the critical parameters are expected to be different at temperatures above the dew point of sodium sulfate, attempts were made to reproduce the recommended VAMAS conditions for this study, albeit at a higher temperature. A 0.98% sulfur fuel was fed into the burner rig at 72 cm^3 h^{-1}, artificial sea water (ASTM D1141)[18] was diluted by a factor of 4 and injected at a rate equivalent to 132 mg h^{-1} of Na, and air was fed at 1500 l h^{-1}. This gave the conditions listed in Table 2. It should be noted that the deposition rate at 900°C for condition 1 is 2·5 times that reported by Laboratory 1 in Ref. 17. However, from experience in our laboratory, the difference is within experimental error. The standard deviation of 10 deposition measurements was 26·7 $\mu g\ cm^{-2}\ h^{-1}$ for a mean of 56 $\mu g\ cm^{-2}\ h^{-1}$.

Table 1. Composition of corrosion samples (wt%)

Material	Si_3N_4	Y_2O_3	Al_2O_3
Material A	88·65	6·95	4·5

Prior to exposure, all samples were ground to a 1 μm finish and had a variability of section along their length of <5μm. All samples were measured using a micrometer calibrated to 1μm which gave a reproducibility of ±1 μm on 12 repeat measurements of the same sample.

After exposure, samples were carefully sectioned perpendicular to the long axis, polished to 1 μm and measured for non-corroded cross-section using a projection microscope calibrated to ±5 μm. Each sample was measured at several points along its length and up to 20 measurements were made of each section with the intention of providing sufficient data for detailed statistical analysis.

Results

Weight change measurements of material A exposed in the burner rig at 1300°C are shown in a parabolic rate plot in Fig. 2. It can be seen from this graph that the corrosion does not follow the same parabolic rate law for the duration of the experiment, and that there is a significant decrease in the parabolic rate constant at longer times. This type of behaviour has been observed by other workers[21,22] and has been proposed to be caused by precipitation of crystalline phases, such as cristobalite or yttrium disilicate, at the scale–ceramic interface thereby inhibiting diffusion. Figure 3 shows yttrium disilicate precipitates in the glassy scale formed on a sample that had been exposed in the burner rig for 480 h. The distribution of the precipitates does not suggest that they would be an effective diffusion barrier, therefore the explanation of the change in rate law must lie elsewhere.

The average section loss for material A exposed at 1300°C is plotted in Fig. 4 as a function of distance from the base of the sample at different

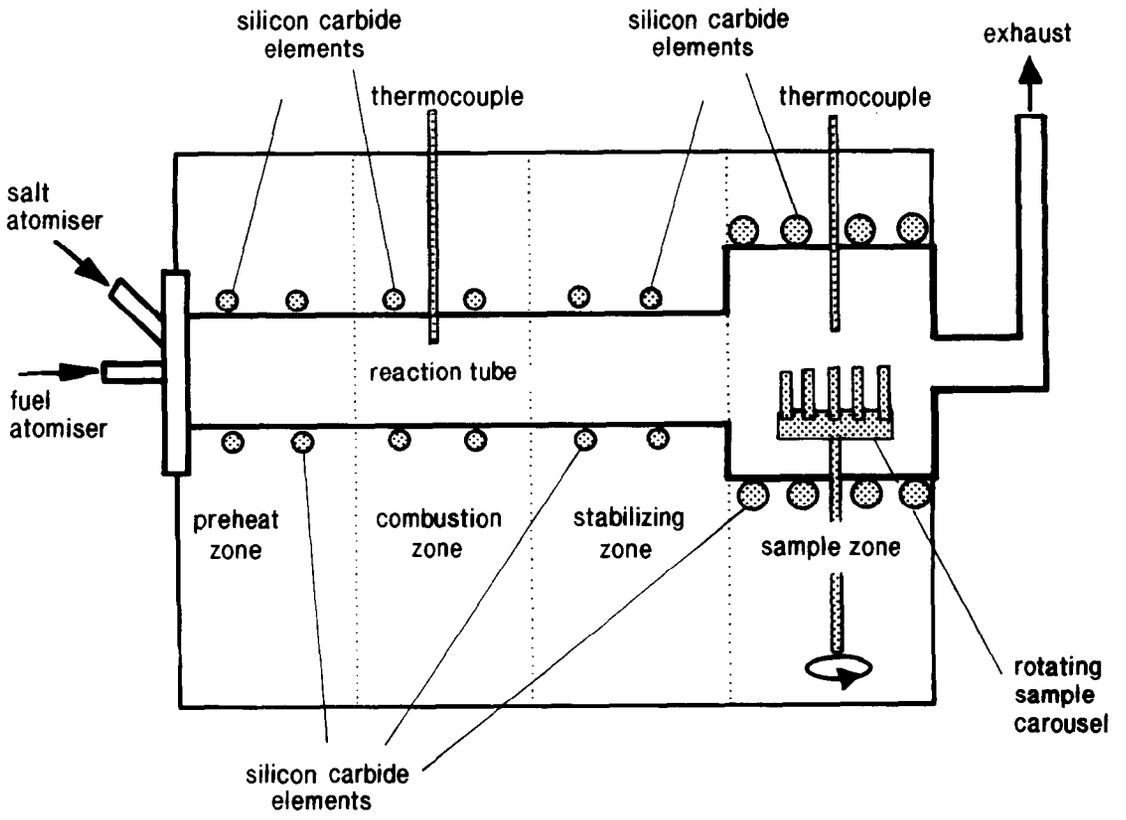

Fig. 1. Schematic diagram of burner rig.

exposure times. It is clear from this figure that there is a significant change in rate of attack along the length of each specimen. There are very obvious differences at each end of the sample, at the base due to interaction with the carousel, and also at the top. This type of variation in attack is also found in burner rig corrosion of superalloys and is accommodated by avoiding taking measurements close to the sample ends. However, in the present case, there is clearly a systematic change in attack along the central portion of the sample, making it impossible to combine the raw data to create a single data set.

The change in rate of attack along the sample length can be attributed to the relatively fluid scales that are formed under the present conditions. Scale formed at the top of the sample is inclined to creep towards the bottom over the duration of the experiment, causing thickening of the scale lower down the sample and thinning of the scale at the top. This in turn leads to inhibition of corrosion lower in the sample and acceleration towards the top. Visual observations of scale thickness are in accord with the proposed mechanism. Regardless of the cause of variation, the difficulty in the present case lies in defining a 'representative' rate of attack. It seems reasonable that the representative rate occurs at the point along the sample where the scale thickness is equal to that which would exist if no creep had occurred. In the present case this point is defined as the mid point of the central portion of the sample, i.e. the portion of the sample unaffected by end effects. This definition still presents a problem in that, in each of the samples measured, this point does not correspond to a measurement point; also, it would be desirable to measure at more than one point in order to build up a large enough data set. In order to make use of data already obtained, and to allow the use of multiple measurement points in the future, a normalization procedure was adopted. This procedure calculated the magnitude that each measurement would have, if it had originated from the middle of

Table 2. Burner rig conditions

Condition	p_{Na_2O} *(atm)*	p_{SO_3} *(atm)*	p_{O_2} *(atm)*	*Na CFR* *(g cm^{-2} h^{-1})*	*Na_2SO_4 deposition rate (at 900°C) (μg cm^{-2} h^{-1})*
Condition 1	$1{\cdot}3 \times 10^{13}$	$2{\cdot}3 \times 10^{6}$	$9{\cdot}7 \times 10^{2}$	$3{\cdot}6 \times 10^{3}$	56

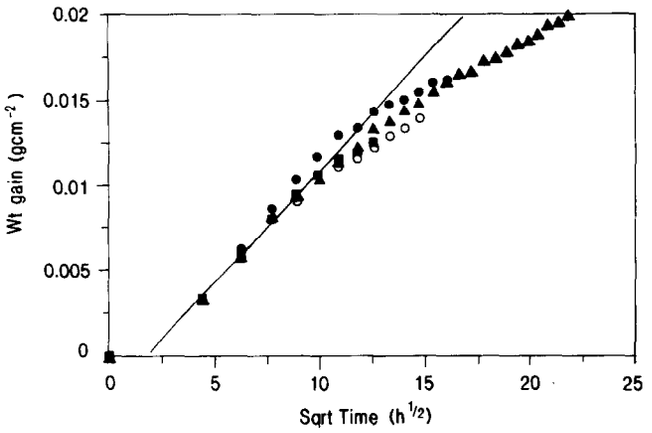

Fig. 2. Parabolic rate plot for material A exposed in the burner rig at 1300°C, atmospheric condition 1. (Different symbols indicate different samples of the same material.)

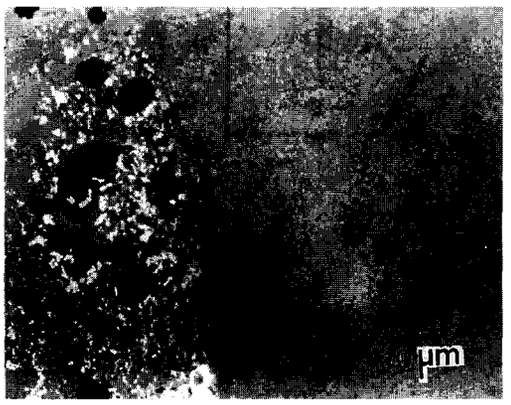

Fig. 3. Scanning electron micrograph of the corrosion scale showing the distribution of yttrium disilicate particles (white phase).

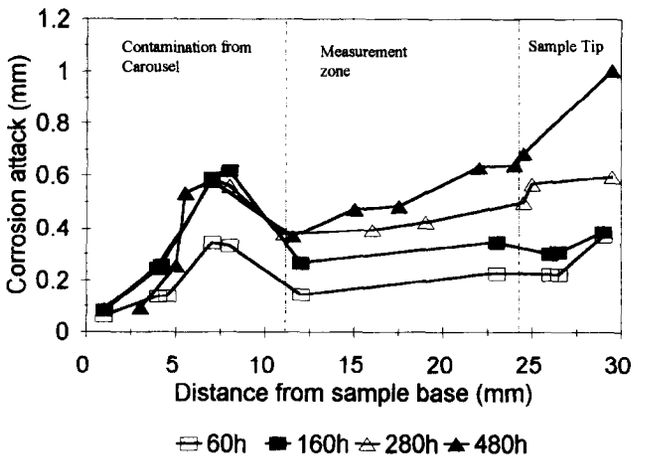

Fig. 4. Average section loss of material A as a function of distance from the sample base, after exposure in the burner rig for 60 h, 160 h, 280 h and 480 h.

the centre zone. The normalizing procedure is described in detail in the Appendix. Figure 5 shows a normal probability plot for the combined data set for 480 h exposure, generated using the normalizing procedure. It is clear that the data give a good fit to a single normal distribution. The

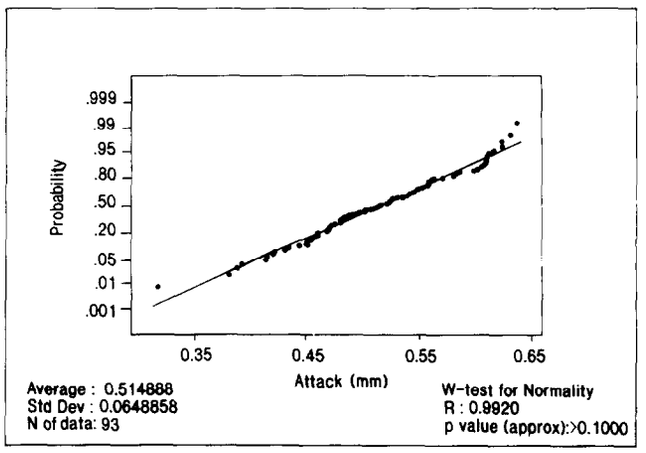

Fig. 5. Normal probability plot of section loss data for material exposed in the burner rig for 480 h. Data from multiple sections pooled using normalization procedure and plotted as attack in mm.

same procedure yielded similar results for measurements after 60, 160 and 280 h exposure, and the mean and standard deviation of the combined data set for each exposure time are given in Table 3.

It is generally the maximum corrosion rather than the average that causes component failure. Extreme value statistics were used to evaluate the data in the present study. Employing the method proposed by Nicholls and Hancock,[20] the top 10% of each normalized data set was analysed using the Type 1 extreme value model of maxima. The cumulative distribution function for this model is given in the following equation:

$$F_1(x_e) = \exp\left\{-\exp\left[-\left(\frac{x_e - \mu_e}{\sigma_e}\right)\right]\right\} \quad (1)$$

where x_e is an extreme value of corrosion loss, μ_e is the extreme value location parameter which corresponds to the most likely extreme value and σ_e is the extreme value scale parameter.

Table 3 shows the extreme value parameters μ_e and σ_e determined at each exposure time. μ_e^2 and σ_e are plotted as a function of time in Fig. 6. It is clear from this figure that the location parameter follows a parabolic relationship with time and the scale parameter is independent of time:

$$\mu_e^2 = 7{\cdot}97 \times 10^{-4}\, t \quad \text{(mm)} \quad (2a)$$

$$\sigma_e = 0{\cdot}02 \quad \text{(mm)} \quad (2b)$$

This result contrasts with that for weight gain measurements, in that a single parabolic relationship describes the increase in μ_e as a function of time whereas the parabolic rate constant for weight change decreases at longer times. If this change does relate to a change in corrosion mechanism, it would be expected to appear in the section loss data. However, it should be borne in mind that weight gain assesses the entire sample,

Table 3. Mean and extreme depth of attack as a function of exposure time

Exposure time (h)	*Mean depth of attack (mm)*	*Standard deviation of depth of attack*	μ_e *(mm)*	σ_e *(mm)*
60	0·188	0·024	0·223	0·010
160	0·310	0·028	0·342	0·042
280	0·417	0·040	0·486	0·017
480	0·515	0·065	0·615	0·011

including the anomalous regions at the sample ends, and the differences in the two methods of measurement may be related to this or to the creep of scale to the bottom of the sample. Regardless of the reason for the discrepancy between weight gain and section loss measurements, it serves as an excellent illustration of the dangers of placing too much emphasis on weight change data.

Probability of corrosion exceeding a certain value

It is possible to use the extreme value distribution to calculate the probability of corrosion penetration exceeding a certain value, and thereby, if a critical depth of penetration can be defined, calculate the probability of failure. The probability Q_1 of extreme corrosion exceeding a certain value x_e, is given by:

$$Q_1 = 1 - \exp\left[-\exp\left(-\frac{(x_e - \mu_e)}{\sigma_e}\right)\right] \quad (3)$$

Employing the time-dependent expression for μ_e and σ_e derived above we obtain

$$Q_1 = 1 - \exp\left[-\exp\left(-\frac{(x_e - 2{\cdot}8 \times 10^{-2}\, t^{1/2})}{0{\cdot}02}\right)\right] \quad (4)$$

The probability of extreme corrosion exceeding a particular value, x_e, has been calculated using eqn (4) for 480, 1000 and 10000 h exposure and is plotted in Fig. 7. If we decide on an acceptable risk, for example one in one thousand, of corrosion exceeding a critical value, we can then use Fig. 7 to predict the likely extreme value of corrosion and, if this value exceeds that for corrosion failure, we can assume that the component would fail within the given time.

As we have defined extreme corrosion as being the top ten percentile of the measured data, the probability Q of any corrosion exceeding a value x_e is given by:

$$Q = \frac{Q_1}{10}$$

$$\therefore Q = \frac{1}{10}\left\{1 - \exp\left[-\exp\left(-\frac{(x_e - 2{\cdot}8 \times 10^{-2}\, t^{1/2})}{0{\cdot}02}\right)\right]\right\} \quad (5)$$

Comparison with data for superalloys

In their recent report of the VAMAS round robin on superalloy testing in burner rigs, Saunders and Nicholls reported results of tests at 900°C.[17] This temperature is getting close to the top end of metal surface temperatures in metallic gas turbines, and it is an appropriate comparison for ceramics under the current conditions which are at the high end of likely temperatures for ceramic gas turbines. Saunders and Nicholls reported the most extreme value from 72 radial measurements, therefore the probability of exceedance of the most extreme observation is 1·4%. In order for the present results to be comparable with this, the

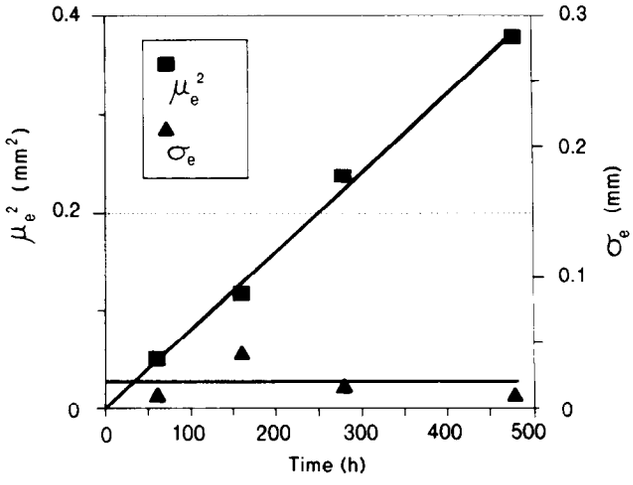

Fig. 6. Extreme value parameters μ_e and σ_e plotted as a function of time.

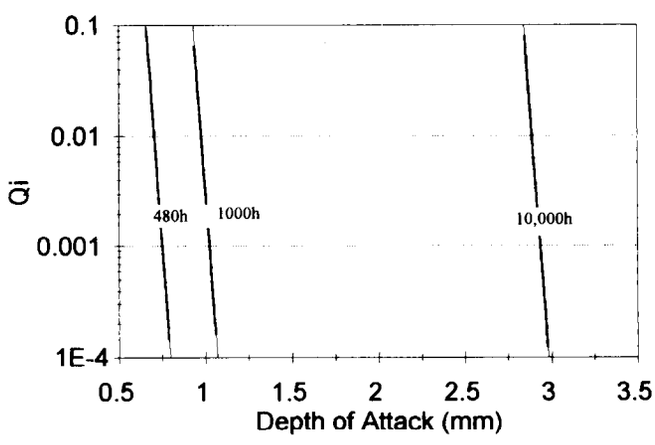

Fig. 7. The probability, Q_1, of extreme corrosion exceeding a particular depth of attack x_e, plotted as a function of x_e.

most extreme value should be the highest 1·4% of the sample of measurements. In this case, we have determined the most likely extreme value where it is the highest 10% of a single sample of corrosion measurements. If we took seven such samples, the most extreme of all the extremes would represent 1·4% of all measurements. Using the reproductive property of the extreme value distribution[20,23] we can calculate the most probable maximum extreme, $\mu_{e,e}$, from n extreme values:

$$\mu_{e,e} = -\mu_e + \sigma_e \ln(n) \quad (6)$$

and, if we use our time-dependent correlation,

$$\mu_{e,e} = 2{\cdot}8 \times 10^{-2} t^{1/2} + 0{\cdot}02 \ln(n) \quad (7)$$

Table 4 shows the most likely maximum, of seven extreme corrosion measurements for the present material, compared with the maximum observed corrosion from 72 measurements for superalloys corroded in an identical burner rig at similar conditions at 900°C. The ceramic materials performed better than the uncoated superalloys but not as well as the coated materials. It should be noted that the corrosion penetration for the sialon followed a parabolic rate law whereas most data on hot corrosion of superalloys suggest a linear corrosion rate law. This would improve the relative performance of the ceramic materials at longer times. Figure 8 shows a plot of most likely maximum extreme corrosion as a function of time, calculated using eqn (3), for seven and 1000 extreme data points. Measured data from the present study and measured and predicted data for IN738LC are included for comparison. This shows that even when the probability of exceedance is less than one in ten thousand the most likely maximum extreme corrosion for the ceramic material is less than that measured for IN738LC and that the difference is expected to increase with time.

Despite the remarkably good fit of the pooled data to both normal and extreme value distributions, care should be taken when making comparisons and extrapolating to longer times. The VAMAS conditions were chosen for superalloy testing because of their aggressive nature towards

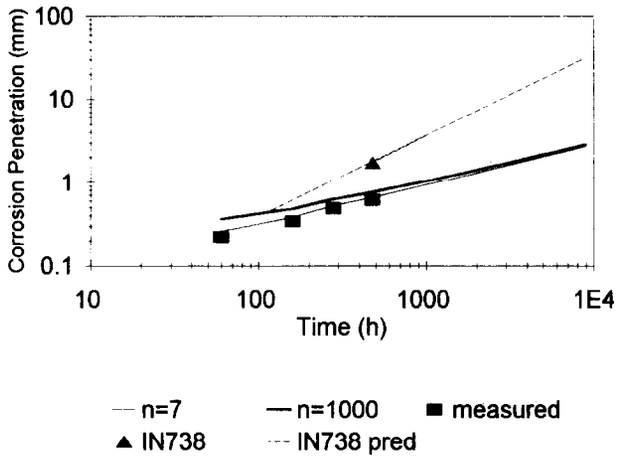

Fig. 8. The most likely maximum extreme corrosion penetration plotted as a function of time and number, n, of extreme data points. (Data for superalloys and measurements from the current work are included for comparison.)

superalloys, i.e. high sulfur atmospheres. Changes to lower sulfur fuels are likely to cause less corrosion of superalloys but appear to cause more for silicon-based ceramics.[10,19] There is also no guarantee that the parabolic relationship found for sialon up to 500 h would continue for longer times. However, despite these misgivings, the sialon studied in this investigation is comparable with superalloys, in terms of corrosion performance, when both types of material are studied at the upper limits of their temperature range, and is worthy of further study to determine the magnitude of the effect of changing the combustion atmosphere.

Conclusion

(1) Samples of sialon corroded in a simulated gas turbine atmosphere show a systematic variation in corrosion from top to bottom of the sample. This variation can cause problems in determining a representative value for the extent of corrosion, but the difficulty can be overcome by normalizing the data relative to an appropriate fixed point on the sample.

Table 4. Comparison of maximum observed corrosion for superalloys with predicted maximum for the current material under similar atmospheric conditions

Material	*Exposure temperature and time*	*Maximum corrosion penetration (mm)*
Sialon (this study)	1300°C, 480 h	0·65 (predicted)
In738LC (VAMAS round robin)	900°C, 500 h	1·8
In738LC/RT22 coating (VAMAS round robin)	900°C, 500 h	0·12
Rene 80 (VAMAS round robin)	900°C, 500 h	>3
Rene 80/ATD2B coating (VAMAS round robin)	900°C, 500 h	0·03

(2) Normalized data from several sample cross-sections can be pooled and the maximum top 10% of the pooled data can be analysed using extreme value statistics.
(3) The extreme value parameters μ_e and σ_e have been correlated with time and used to predict corrosion behaviour at longer times.
(4) Comparison of extreme corrosion predicted from the present study, with measurements of superalloys corroded under identical conditions at 900°C, shows that the sialon material outperforms uncoated superalloys. However, care must be taken when making these comparisons, particularly where time extrapolation is concerned.

Acknowledgements

The authors are indebted to International Syalons for supplying materials and EPSRC for funding this research.

References

1. Jacobson, N. S., *J. Am. Ceram. Soc.*, **76** (1993) 3.
2. Parker, D. A., *Met. Mater.*, **6** (1990) 14.
3. Nishikita, A., Numata, H. & Tsuru, T., *Mater. Sci. Eng.*, **A146** (1991) 15.
4. Rapp, R. A., *Mat. Sci. Eng.*, **87** (1987) 319.
5. Stringer, J., *Mat. Sci. Technol.*, **3** (1987) 482.
6. Jacobson, N. S. & Fox, D. S., *J. Am. Ceram. Soc.*, **71** (1988) 139.
7. Mayer, M. I. & Riley, F. L., *J. Mater. Sci.*, **13** (1978) 1319.
8. Pareek, V. & Shores, D. A., *J. Am. Ceram. Soc.*, **69** (1991) 556.
9. Jacobson, N. S., Stearns, C. A. & Smialek, J. L., *Adv. Ceram. Mater.*, **1** (1986) 145.
10. G-Ahari, K., Coley, K. S., Baxter, D. J. & Hendry, A., In *Advances in Science and Technology 9: High Performance Materials in Engine Technology*, ed. P. Vicinzini. Techna Publications, 1995, p. 411.
11. Booth, G. C. & Clarke, R. L., *Mater. Sci. Technol.*, **2** (1986) 272.
12. Saunders, S. R. J. & Nicholls, J. R., *Thin Solid Films*, **119** (1984) 247.
13. Hot Corrosion Task Force Panel, ASTM Round Robin Test, 1970.
14. Hancock, P., *Corros. Sci.*, **22** (1982) 51.
15. Saunders, S. R. J., Hossain, M. K. & Fergouson, J. M. In *High Temperature Alloys for Gas Turbines 1982*, eds R. Brunetaud *et al.* D. Reidel Publishing Co., Dordrecht, 1982, p. 177.
16. Nicholls, J. R. & Saunders, S. R. J., *High Temp. Technol.*, **7** (1989) 193.
17. Saunders, S. R. J. & Nicholls, J. R., Hot salt corrosion testing—an international intercomparison. *Mater. High Temp.*, to be published.
18. Saunders, S. R. J. & Nicholls, J. R., *High Temp. Technol.*, **7** (1989) 232.
19. G-Ahari, K., Coley, K. S., Graziani, T. & Baxter, D. J., work to be published.
20. Nicholls, J. R. & Hancock, P. In *Plant Corrosion Prediction of Materials Peformance*, eds J. E. Strutt & J. R. Nicholls. Ellis Horwood, Chichester, 1987, p. 257–273.
21. Nickel, K. G., Danzer, R., Schnieder, G. & Petzow, G., *Powder Metall. Int.*, **21**[3] (1989) 29.
22. Persson, J., Kall, P.-O. & Nygren, M., *J. Am. Ceram. Soc.*, **75**[12] (1992) 3377.
23. Bury, K. V., *Statistical Models in Applied Science*, John Wiley and Sons Inc., New York, 1975.

Appendix: Normalization Procedure with respect to Height from Sample Base

In order to obtain a sufficiently large data set from burner rig samples, it is often necessary to combine measurements taken from different points along the sample length. However, in the present work there was some difficulty in doing this because of the systematic variation in measured corrosion along the sample length. Inspection of Fig. A1, for a sample corroded for 480 h, reveals that the variation follows a linear relationship in the portion of the sample that is not prone to 'end effects'. Therefore, if we can define a representative point along the sample length, it should be possible to calculate the magnitude of corrosion at this point from measurements at another by employing that relationship. As the reason for the variation appears to be creep of the scale from the top to the base of the sample, the representative point should be that which has experienced no thickening or thinning of the scale due to creep. In the present work the 'no creep condition' was assumed to occur at the midpoint of the central portion of the sample, i.e. 18 mm from the sample base.

Having defined the representative point, all data from the central portion of the sample were normalized with respect to this point. The procedure adopted is illustrated in Fig. A1 by considering data points 1 and 2, which are average values of all measurements obtained at point 1 and point 2. For example, consider a measurement x_1 contributing to the average plotted at point 1, this undergoes translation along the solid diagonal line

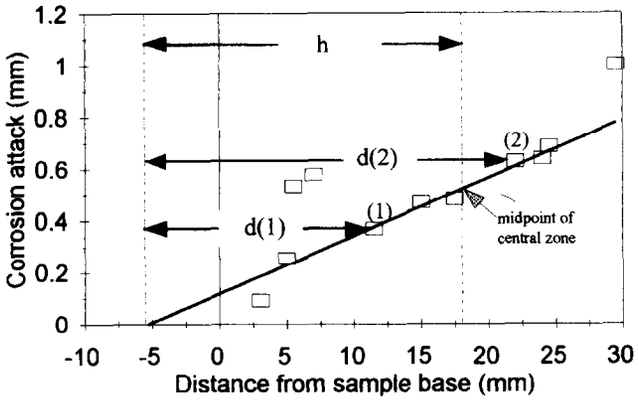

Fig. A1. Average section loss as a function of distance from sample base illustrating normalization procedure.

to the representative point where it will have the value $x_{r,1}$ The value of $x_{r,1}$ is given by:

$$x_{r,1} = x_1 \frac{h}{d(1)} \quad \text{(A1)}$$

A similar procedure can be adopted for a measurement contributing to data point 2, where the new value, $x_{r,2}$, is given by:

$$x_{r,2} = x_2 \frac{h}{d(2)} \quad \text{(A2)}$$

When this procedure was used to normalize all corrosion measurements from the centre portion of a sample, the resulting data set could be represented by a single normal distribution (see Fig. 5). This distribution has been assumed to be representative of the sample where the scale is in the 'no creep' condition. An identical approach has been used to pool data for multiple cross-sections of each sample in the present investigation.